INTERNATIONAL JOURNAL FOR NUMERICAL METHODS IN FLUIDS
Int. J. Numer. Meth. Fluids 2000; **32**: 881–897

On a higher-order bounded discretization scheme

B. Song[a], G. R. Liu[a], K. Y. Lam[a] and R. S. Amano[b,*]

[a] *Institute of High Performance Computing, # 01-05/08 The Rutherford, Singapore 118261, Singapore*
[b] *Department of Mechanical Engineering, University of Wisconsin-Milwaukee, Milwaukee, WI 53201, U.S.A.*

SUMMARY

This paper presents a new higher-order bounded scheme, weighted-average coefficient ensuring boundedness (WACEB), for approximating the convective fluxes in solving transport equations with the finite volume difference method (FVDM). The weighted-average formulation is used for interpolating the variables at cell faces and the weighted-average coefficient is determined from normalized variable formulation and total variation diminishing (TVD) constraints to ensure the boundedness of solution. The new scheme is tested by solving three problems: (1) a pure convection of a box-shaped step profile in an oblique velocity field, (2) a sudden expansion of an oblique velocity field in a cavity, and (3) a laminar flow over a fence. The results obtained by the present WACEB are compared with the UPWIND and the QUICK schemes and it is shown that this scheme has at least second-order accuracy, while ensuring boundedness of solutions. Moreover, it is demonstrated that this scheme produces results that better agree with the experimental data in comparison with other schemes. Copyright © 2000 John Wiley & Sons, Ltd.

KEY WORDS: boundedness; discretization scheme; weighted-average

1. INTRODUCTION

The approximation of the convection fluxes in the transport equation has a decisive influence on the overall accuracy of any numerical solution for fluid flow and heat transfer. Although convection is represented by a simple first-order derivative, its numerical representation remains one of the central issues in computational fluid dynamics (CFD). The classical first-order schemes, such as UPWIND, HYBRID, POWER-LAW, are unconditionally bounded, but tend to misrepresent the diffusion transport process through the addition of numerical or 'false' diffusion arising from flow-to-grid skewness. The higher-order schemes, such as the second-order upwind [1] and the third-order upwind (QUICK) [2], offer a rout to improve accuracy of the computations. However, they all suffer from the boundedness problems; i.e. the solutions may display unphysical oscillations in regions of steep gradients, which can be sufficiently serious to cause numerical instability.

* Correspondence to: Department of Mechanical Engineering, College of Engineering and Applied Science, University of Wisconsin-Milwaukee, PO Box 784 EMS, Milwaukee, WI 53201, U.S.A.

Received 1 June 1998
Revised 30 June 1999

During the last decade, efforts have been made to derive higher resolution and bounded schemes. Zhu and Leschnizer [3] proposed a local oscillation-damping algorithm (LODA). Since the LODA scheme introduces the contribution of the upwind scheme, the second-order diffusion is introduced into those regions where QUICK displays unbounded behavior. In 1988, Leonard [4] developed a normalized variable formulation and presented a high resolution bounded scheme named SHARP (simple high-accuracy resolution program). Gaskell and Lau [5] developed a scheme called SMART (sharp and monotonic algorithm for realistic transport), which employs a curvature compensated convective transport approximation and a piecewise linear normalized variable formulation. However, the numerical testing [6] shows that both SMART and SHARP need an underrelaxation treatment at each of the control volume cell faces in order to suppress the oscillatory convergence behavior. This drawback leads to an increase of the computer storage requirement, especially for three-dimensional flow calculation. In 1990, Zhu [7] proposed a hybrid linear/parabolic approximation scheme (HLPA). However, this method has only the second-order accuracy.

In the present study, a weighted-averaged formulation is employed to interpolate variables at cell faces and the weighted-average coefficient will be determined based on the normalized variable formulation and total variation diminishing (TVD) constraints. Three test cases are examined: (1) a pure convection of a box-shaped step profile in an oblique velocity field, (2) a sudden expansion of an oblique velocity field in a cavity, and (3) laminar flow over a fence. Computations were performed on a generalized curvilinear co-ordinate system. The schemes are implemented in a deferred correction approach. The computed results are compared with those obtained using QUICK and UPWIND schemes and available experimental data.

2. NUMERICAL FORMULATION

2.1. Governing equations

The conservation equations governing incompressible steady flow problems are expressed in the following general form:

$$\operatorname{div} \lfloor \rho \vec{V} \Phi - \Gamma_\Phi \operatorname{grad}(\Phi) \rfloor = S_\Phi \tag{1}$$

where Φ is any transport variable, $\vec{V}$ is the velocity vector, ρ is the density of the fluid, Γ_Φ is the diffusive coefficient and S_Φ denotes the source term of variable Φ.

With ξ, η, ζ representing the general curvilinear co-ordinates in a three-dimensional framework, the transport equation (1) can be expressed as

$$\begin{aligned}&\frac{1}{J}\left[\frac{\partial \rho U \Phi}{\partial \xi}+\frac{\partial \rho V \Phi}{\partial \eta}+\frac{\partial \rho W \Phi}{\partial \zeta}\right]\\&=\frac{1}{J}\frac{\partial}{\partial \xi}\left[\frac{\Gamma_\Phi}{J}\left(q_{11}\Phi_\xi\right)\right]+\frac{1}{J}\frac{\partial}{\partial \eta}\left[\frac{\Gamma_\Phi}{J}\left(q_{22}\Phi_\eta\right)\right]+\frac{1}{J}\frac{\partial}{\partial \zeta}\left[\frac{\Gamma_\Phi}{J}\left(q_{33}\Phi_\zeta\right)\right]+S^{\mathrm{CD}}+S_\Phi(\xi,\eta,\zeta)\end{aligned} \tag{2}$$

where U, V and W are the contravariant velocities defined by

$$U = j_{11}u + j_{21}v + j_{31}w \tag{3a}$$

$$V = j_{12}u + j_{22}v + j_{32}w \tag{3b}$$

$$W = j_{13}u + j_{23}v + j_{33}w \tag{3c}$$

and J is the Jacobian, q_{ij} and j_{ij} ($i = 1$–3 and $j = 1$–3) are the transformation coefficients (given in Appendix B), S^{CD} is the cross-diffusion term (referred to in Appendix B).

2.2. Discretization

The computational domain is uniformly divided into hexahedral control volumes and the discretization of transport equation (2) is performed in the computational domain following the finite volume method.

Integrating Equation (2) over a control volume as shown in Figure 1 and applying the *Gauss Divergence Theorem* in conjunction with central difference for diffusion, we have

$$F_e - F_w + F_n - F_s + F_t - F_b = S_\Phi \Delta V + S^{CD} \Delta V \tag{4}$$

where F_f represents the total fluxes of Φ across the cell face f (f = e, w, n, s, b, t). Taking the east face as an example, the total fluxes across it can be written as

$$F_e = (\rho U \Phi)_e - \left(\frac{\Gamma^\Phi}{J} q_{11}\right)_e (\Phi_E - \Phi_P) \tag{5}$$

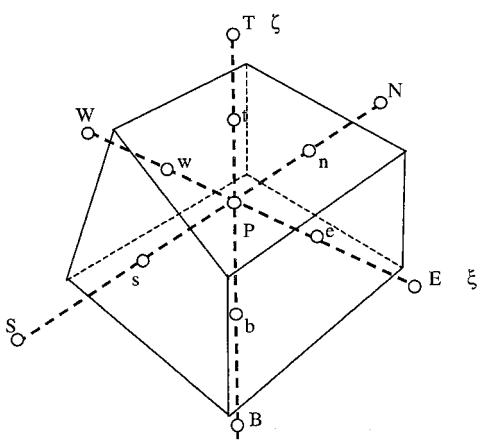

Figure 1. A typical control volume.

In the above equation, the cell face values of Φ can be approximated with different schemes.

For the first-order UPWIND scheme, the cell face value is expressed as

$$\begin{aligned} \Phi_e &= \Phi_P \quad \text{if } U_e > 0 \\ \Phi_e &= \Phi_E \quad \text{if } U_e < 0 \end{aligned} \tag{6}$$

Upon substitution of Equations (5) and (6) into Equation (4), we have

$$A_P \Phi_P = \sum_{i=\mathrm{E,W,N,S,T,B}} A_i \Phi_i + S_C \tag{7}$$

where the subscript i denotes neighboring grid points, A_P and A_i are the coefficients relating to the convection and diffusion and S_C is the source term.

2.3. Higher-order schemes

The approximation of convection has a decisive influence on the overall accuracy of the numerical simulations for a fluid flow. The first-order schemes such as UPWIND, HYBRID and POWER-LAW all introduce the second-order derivatives that then lead to falsely diffusive simulated results. Therefore, the higher-order schemes have to be used to increase the accuracy of the solution. Generally, with uniform grid spacing, the higher-order interpolation schemes can be written as in the following weighted-average form:

$$\begin{aligned} \Phi_e &= \underline{\Phi_P} + \frac{1}{4}[(1-\kappa)\Delta_e^- + (1+\kappa)\Delta_e] \quad \text{if } U_e > 0 \\ \Phi_e &= \underline{\Phi_E} - \frac{1}{4}[(1-\kappa)\Delta_e^+ + (1+\kappa)\Delta_e] \quad \text{if } U_e < 0 \end{aligned} \tag{8}$$

where

$$\Delta_e^- = \Phi_P - \Phi_W, \quad \Delta_e = \Phi_E - \Phi_P, \quad \Delta_e^+ = \Phi_{EE} - \Phi_E$$

and where κ is the weighted-average coefficient. In Equation (8), the underlined terms represent the fragments of the first-order upwind scheme. Therefore, the higher-order schemes can be implemented in a deferred correction approach proposed by Khosla and Rubin [8], that is

$$\Phi_f^{n+1} = \Phi_f^{\mathrm{UP},n+1} + (\Phi_f^{\mathrm{HO},n} - \Phi_f^{\mathrm{UP},n}) \tag{9}$$

where n indicates the iteration level, UP and HO refer to the upwind and higher-order schemes respectively. The convective fluxes calculated by the upwind schemes are combined with the diffusion term to form the main coefficients of the difference equation, while those resulting from the deferred correction terms are collected into the source term, say S^{DC}. Such a

treatment leads to a diagonally dominant coefficient matrix and enables a higher-order accuracy to be achieved at a converged stage.

With this method, the deferred correction source term, taking east–west direction as an example, is calculated by

$$S^{\mathrm{DC}} = \frac{1}{4}\{U_{\mathrm{e}}^{+}U_{\mathrm{e}}[(1+\kappa)\Delta_{\mathrm{e}} + (1-\kappa)\Delta_{\mathrm{e}}^{-}] - U_{\mathrm{e}}^{-}U_{\mathrm{e}}[(1+\kappa)\Delta_{\mathrm{e}} + (1-\kappa)\Delta_{\mathrm{e}}^{+}] - U_{\mathrm{w}}^{+}U_{\mathrm{w}}[(1+\kappa)\Delta_{\mathrm{w}} + (1-\kappa)\Delta_{\mathrm{w}}^{-}] + U_{\mathrm{w}}^{-}U_{\mathrm{w}}[(1+\kappa)\Delta_{\mathrm{w}} + (1-\kappa)\Delta_{\mathrm{w}}^{+}]\} \tag{10}$$

where $U_{\mathrm{e}}^{\pm}$ is defined as

$$U_{\mathrm{f}}^{\pm} = \frac{1 \pm \mathrm{sgn}(U_{\mathrm{f}})}{2}$$

If κ is fixed at a suitable constant value everywhere, several well-known schemes can be formed, as listed in Table I.

However, the schemes listed in Table I all suffer from a boundedness problem, i.e. the solutions may display unphysical oscillations in regions of steep gradients, which can be sufficiently serious to lead to a numerical instability.

2.4. Weighted-average coefficient ensuring boundedness (WACEB)

Based on the variable normalization proposed by Leonard [4], with a three-node stencil as shown in Figure 2, we introduce a normalized variable defined as

$$\tilde{\Phi} = \frac{\Phi - \Phi_{\mathrm{U}}}{\Phi_{\mathrm{D}} - \Phi_{\mathrm{U}}} \tag{11}$$

where the subscripts U and D represent the upstream and the downstream locations respectively. In the normalized form, the higher-order schemes can be rewritten as

$$\tilde{\Phi}_{\mathrm{f}} = \tilde{\Phi}_{C} + \frac{1}{4}[(1+\kappa)(1-\tilde{\Phi}_{C}) + (1-\kappa)\tilde{\Phi}_{C}] \tag{12}$$

Table I. Typical interpolation schemes.

Scheme	κ	Expression for Φ_{e} when $u>0$	Leading truncation error term
LUDS	-1	$\frac{1}{2}(3\Phi_{\mathrm{P}}-\Phi_{\mathrm{W}})$	$\frac{3}{8}\Delta x^{3}\Phi''$
CD	1	$\frac{1}{2}(\Phi_{\mathrm{E}}+\Phi_{\mathrm{P}})$	$\frac{1}{8}\Delta x^{2}\Phi''$
QUICK	1/2	$\frac{1}{8}(3\Phi_{\mathrm{E}}+6\Phi_{\mathrm{P}}-\Phi_{\mathrm{W}})$	$\frac{1}{16}\Delta x^{3}\Phi'''$
CUI	1/3	$\frac{1}{6}(2\Phi_{\mathrm{E}}+5\Phi_{\mathrm{P}}-\Phi_{\mathrm{W}})$	$-\frac{1}{24}\Delta x^{2}\Phi''$

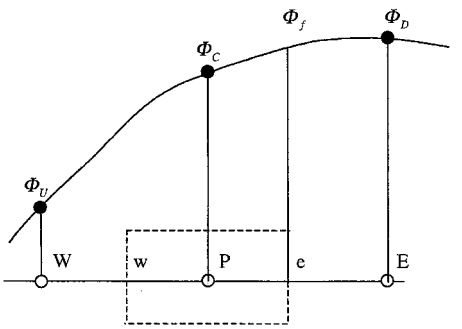

Figure 2. Three-node stencil.

Solving for κ

$$\kappa = \frac{4\tilde{\Phi}_{\mathrm{f}} - 4\tilde{\Phi}_C - 1}{1 - 2\tilde{\Phi}_C} \tag{13}$$

In order to ensure boundedness, the TVD constraints can be used, that is

$$\begin{aligned} &\tilde{\Phi}_{\mathrm{f}} \le 1,\ \tilde{\Phi}_{\mathrm{f}} \le 2\Phi_C,\ \tilde{\Phi}_{\mathrm{f}} \ge \tilde{\Phi}_C \quad \text{for } 0 < \tilde{\Phi}_C < 1 \\ &\tilde{\Phi}_{\mathrm{f}} = \tilde{\Phi}_C \qquad\qquad\qquad\quad \text{for } \tilde{\Phi}_C \le 0 \text{ or } \tilde{\Phi}_C \ge 1 \end{aligned} \tag{14}$$

which correspond to the triangle region shown in Figure 3.

The Taylor serious expansion shows that the first two leading truncation error terms of the interpolation scheme (8) are $\frac{1}{4}(\kappa - \frac{1}{2})\Delta x^2\Phi''$ and $\frac{1}{8}(1-\kappa)\Delta x^3\Phi'''$. Therefore, the scheme has at least second-order accuracy. The maximum accuracy (third-order) can be achieved if κ is set equal to $\frac{1}{2}$. Thus, the scheme can be formed in such a way that κ lies as close to $\frac{1}{2}$ as possible, while satisfying the TVD constraints. Based on this idea, the normalized cell face value can be computed by the following expressions:

$$\tilde{\Phi}_{\mathrm{f}} = \begin{cases} \tilde{\Phi}_C & \tilde{\Phi}_C \notin [0,\ \ 1] \\ 2\tilde{\Phi}_C & \tilde{\Phi}_C \in [0,\ \ 0.3) \\ \frac{3}{8}(2\tilde{\Phi}_C + 1) & \tilde{\Phi}_C \in [0.3,\ \ \frac{5}{6}] \\ 1 & \tilde{\Phi}_C \in (\frac{5}{6},\ \ 1] \end{cases} \tag{15}$$

As shown in Figure 3, the TVD constraints are overly restrictive according to the convection boundedness criterion (CBC). However, using a larger multiplying constant will not noticeably increase the accuracy. The reasons are that, firstly, the constant only affects the accuracy in the range from A to B (see Figure 3) and this range varies at most from 0 to 0.3 (if we use constant

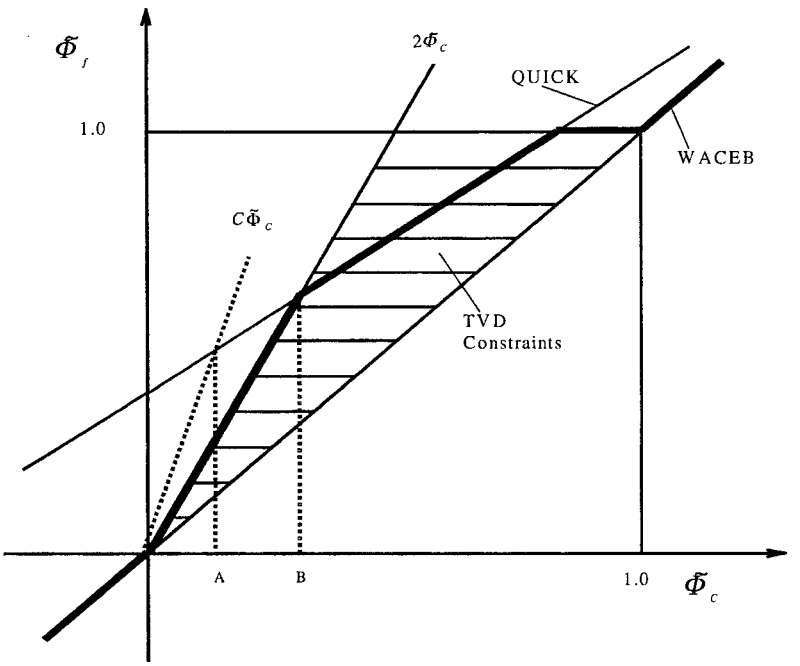

Figure 3. Diagrammatic representation of the TVD constraint and the WACEB scheme.

3, $A = 0.1666$ and $B = 0.3$). Secondly, Even with the smaller constant, the accuracy of the scheme is still second-order. Therefore, the present WACEB scheme uses the normalized variable formulation (15) to calculate the weighted-average coefficient to preserve boundedness.

From Equations (13) and (15), the weighted-average coefficient can be given by

$$\kappa = \begin{cases} 1/(1-2\tilde{\Phi}_C) & \tilde{\Phi}_C \notin [0, \quad 1] \\ (4\tilde{\Phi}_C - 1)/(1-2\tilde{\Phi}_C) & \tilde{\Phi}_C \in [0, \quad 0.3) \\ (3-4\tilde{\Phi}_C)/(1-2\tilde{\Phi}_C) & \tilde{\Phi}_C \in [0.3, \quad \frac{5}{6}] \\ \frac{1}{2} & \tilde{\Phi}_C \in (\frac{5}{6}, \quad 1] \end{cases} \tag{16}$$

The variation of κ with $\tilde{\Phi}_C$ is shown in Figure 4. It is easy to see that the present WACEB scheme satisfies the convective stability condition [2]. It is necessary to mention that the above algorithm is formulated on the assumption of the constant grid spacing. For non-uniform grids, the weighted-average coefficient will also be the function of the grid spacing aspect ratio.

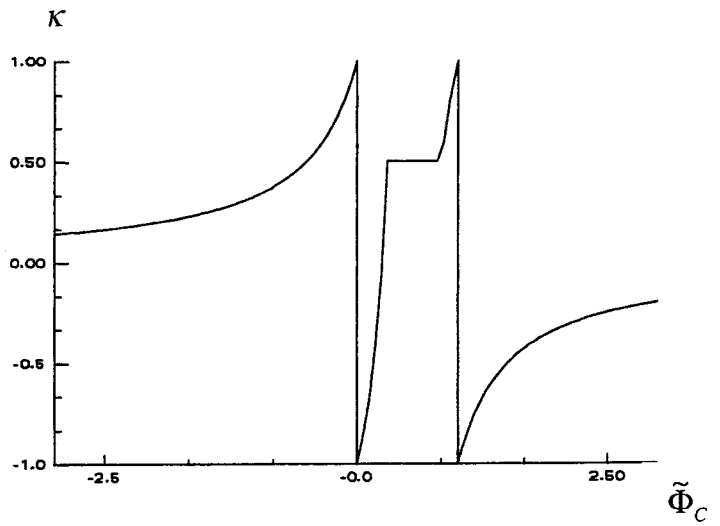

Figure 4. The variation of weighted-average coefficient with a normalized variable.

3. TEST PROBLEM AND RESULTS

The governing transport equations were solved by using the non-staggered finite volume method. A special interpolation procedure developed by Rhie and Chow [9] is used to prevent pressure oscillations due to non-staggered grid arrangement. Pressure and velocity coupling is achieved through the SIMPLE algorithm [10].

It is necessary to mention that QUICK and WACEB schemes all need to employ two upstream nodes for each cell face, which mandates one to involve a value outside the solution domain for a near-boundary control volume. Therefore, an UPWIND scheme is used for all the control volume adjacent to boundaries.

3.1. Pure convection of a box-shaped step profile

The flow configuration shown in Figure 5 constitutes a test problem for examining the performance of numerical approximation to convection because of the extremely sharp gradient in a scalar. This is a linear problem in which the velocity field is prescribed. The calculations are performed with two different uniform meshes, 29×29 and 59×59.

Comparisons of the numerical solutions obtained with the UPWIND, the QUICK and the present WACEB schemes are presented in Figures 6(a) and 6(b). It can be seen that the UPWIND scheme results in a quite falsely diffusive profile for the scalar even with the finer mesh. Although the QUICK scheme reduces such a falsely diffusion, it produces significant overshoots and undershoots. Unlikely, the WACEB predicts a fairly good steep gradient without introducing any overshoots or undershoots. Therefore, we conclude that the WACEB scheme resolves the boundedness problem while reserving a higher-order accuracy.

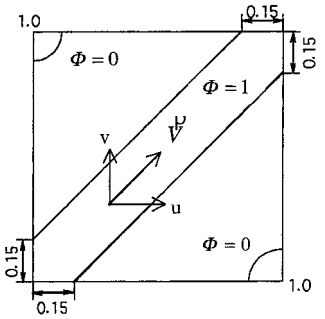

Figure 5. Pure convection of a box-shaped step by a uniform velocity field.

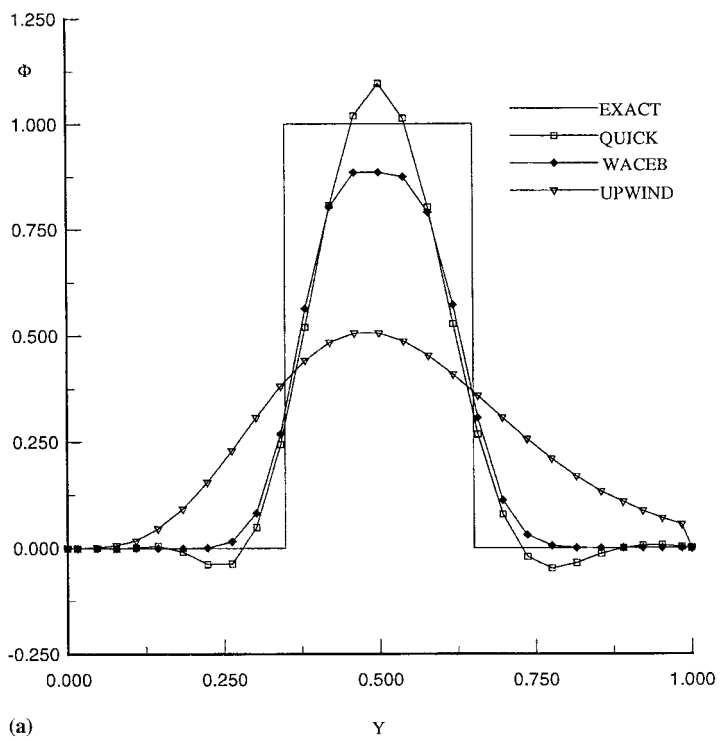

Figure 6. Scalar profiles along the centerline: (a) 29×29, (b) 59×59.

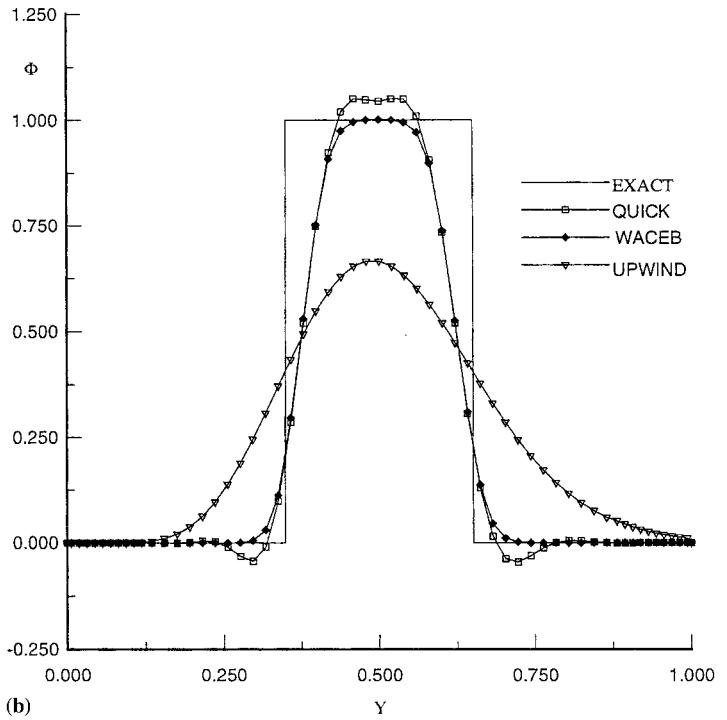

Figure 6 (*Continued*)

3.2. Sudden expansion of an oblique velocity field in a cavity

The geometry under consideration is depicted in Figure 7. The flow is assumed to be steady and laminar. At the inlet, U velocity and V velocity are given a constant value of U_{ref}. The boundary conditions at the outlet are $\partial U/\partial x = 0$ and $\partial V/\partial x = 0$. The calculations are performed on the uniform meshes (59×59). Figure 8 shows the comparison of U velocity along the vertical central lines of the cavity for the Reynolds number of 400. It is observed that the UPWIND scheme cannot predict the secondary recirculation region well, which should appear near the upper-side of the cavity and smears out the steep gradients of the velocity profile near the mainstream. It is also observed that both the WACEB and QUICK schemes do distinctively predict this secondary recirculating region. Furthermore, it is noteworthy to observe that both produce very similar results. The streamline patterns predicted with the three schemes are all shown in Figure 9. It is clearly seen, again, that the UPWIND scheme predicts a much smaller vortex on the left-upper side of the cavity and much wider mainstream region than the QUICK and the WACEB schemes. The computations were further extended to a higher Reynolds number of up to 1000. At this Reynolds number, the QUICK scheme produces a 'wiggle solution'. Figure 10 shows the streamline patterns predicted with the WACEB and the UPWIND schemes. The two schemes give very different flow patterns; with the increase of the

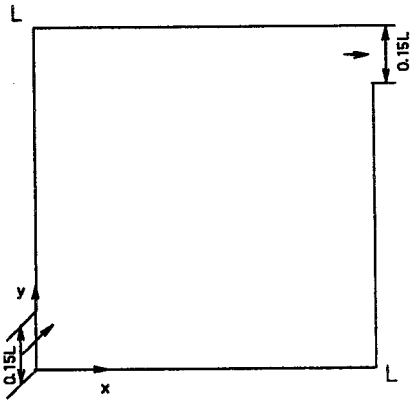

Figure 7. Geometry of a cavity.

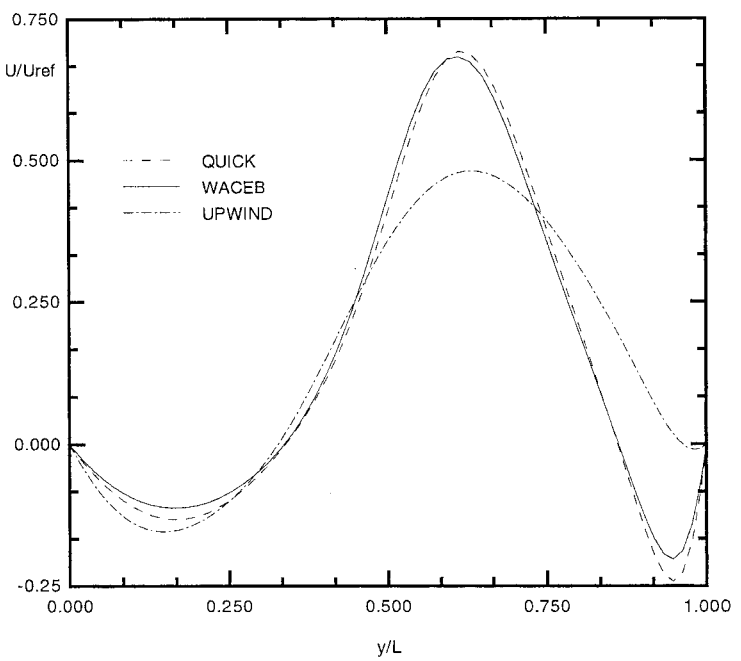

Figure 8. U velocity profile along the vertical centerline of the domain ($Re = 400$).

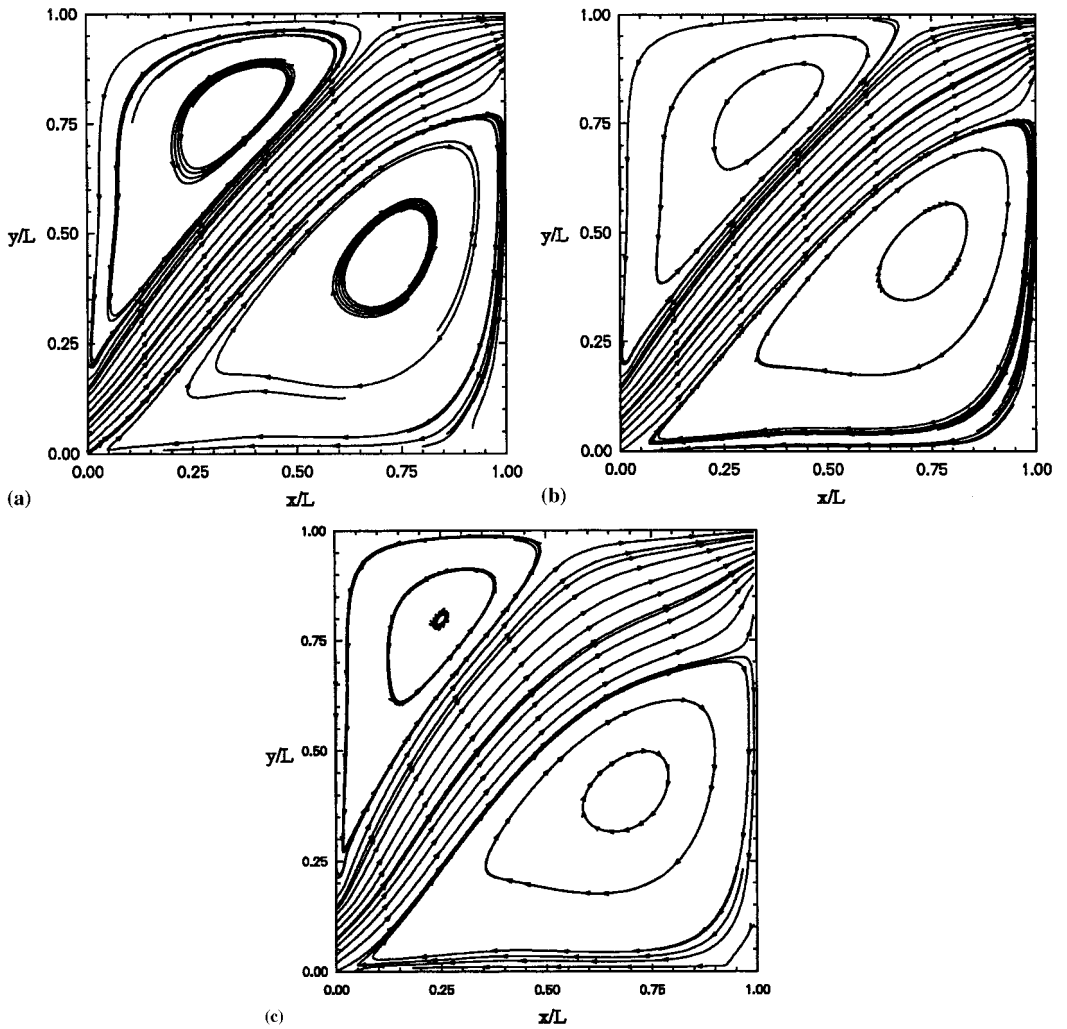

Figure 9. Streamlines for sudden expansion of an oblique velocity field ($Re = 400$): (a) QUICK, (b) WACEB, (c) UPWIND.

Reynolds number, the convection is enhanced and diffusion is suppressed and then the 'dead water regions' should have a less effect on the mainstream region. The results with the WACEB scheme clearly show this trend. It is also noted that the WACEB scheme produces two additional vortices at the two corners of the cavity. However, the UPWIND scheme just predicts a very small additional vortex at the right-lower corner and fails to capture the additional vortex at the left-upper corner.

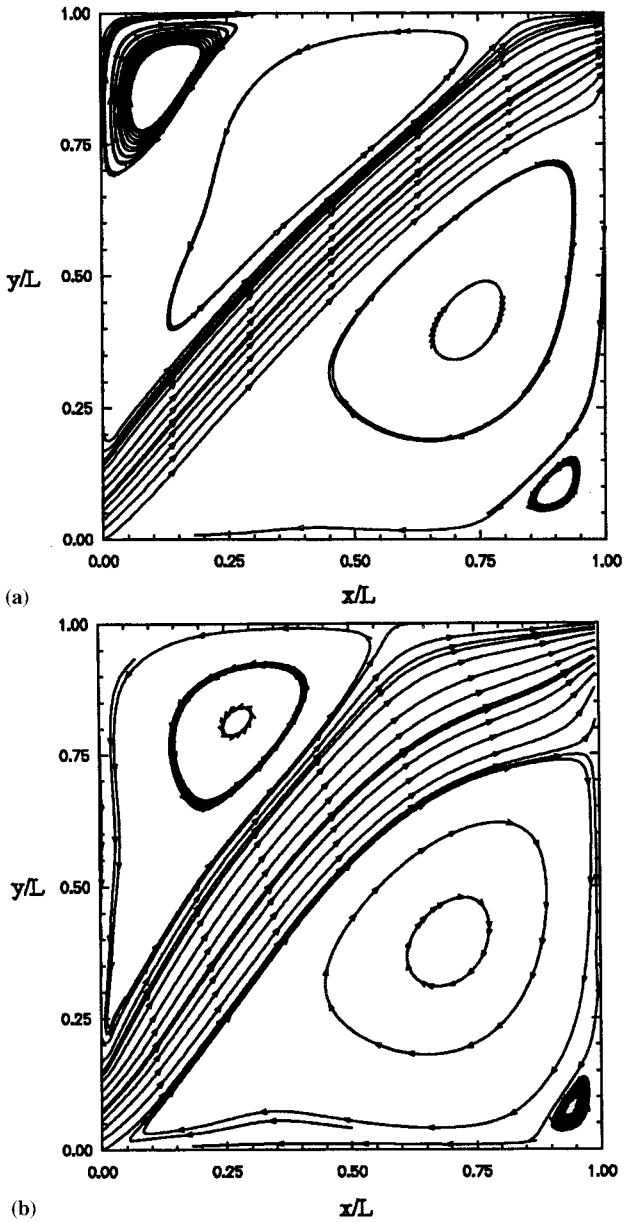

Figure 10. Streamlines for sudden expansion of an oblique velocity field (Re = 1000): (a) WACEB, (b) UPWIND.

From the above discussion, it is concluded that the solution with the WACEB scheme is comparable with that of the QUICK scheme. Even under highly convective conditions, the unbounded QUICK scheme may produce 'wiggle solutions', while the bounded WACEB scheme still produces a reasonable solution.

3.3. Two-dimensional laminar flow over a fence

A two-dimensional laminar flow over a fence, as shown is Figure 11, was studied experimentally by Carvalho [11]. The Reynolds number based on the height of the fence and mean axial velocity is 82.5 and the blockage ratio (s/H) is 0.75. The boundary conditions at the inlet are prescribed as a parabolic profile for the axial velocity U and zero for the cross-flow velocity V. At the outlet, the boundary conditions are given as $\partial U/\partial x = 0$ and $\partial V/\partial x = 0$. The present study shows that the grid-independence results can be achieved with 150×78 uniform meshes for all the schemes.

Figure 12 presents the axial velocity profiles at different locations (x/s) measured [11] and calculated with the QUICK, the WACEB and the UPWIND schemes. We can observe that when x/s is less than 2, the results with the three schemes are nearly identical and are in good agreement with experimental data. However, when x/s is greater than 2, where the second separated flow on the top wall appears, the UPWIND scheme predicts very poor results and the QUICK and the WACEB schemes give very satisfactory results in comparison with the experimental data. These results verify the conclusion drawn from the previous section.

4. CONCLUSIONS

By using normalized variable formulation and TVD constraints, the weighted-average coefficient ensuring the boundedness of the solution is determined and then a bounded scheme is present in this paper. This new scheme is tested for three different flow applications, including a linear convection transport of a scalar, a sudden expansion of an oblique flow field, and a laminar flow over a fence. The numerical tests show that the new WACEB scheme retains the ability of the QUICK to reduce the numerical diffusion without introducing any overshoots or undershoots. The scheme is very easy to implement, stable, free of convergence oscillation and there is no need to incorporate any underrelaxation treatment for weighted-average coefficient calculation.

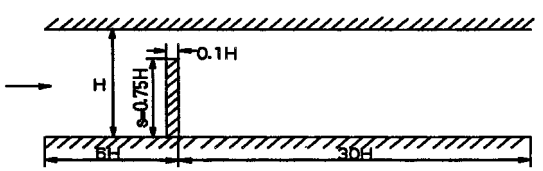

Figure 11. Geometry of flow over a fence.

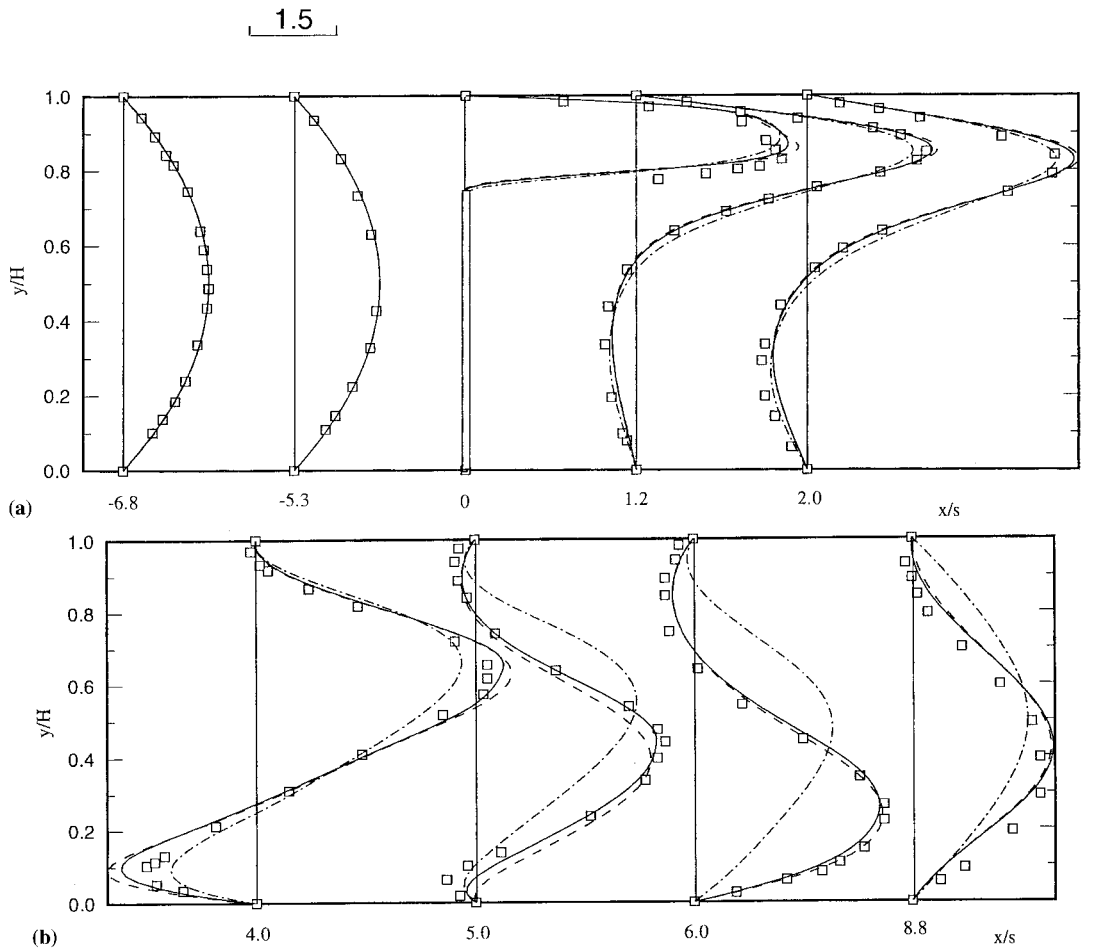

Figure 12. Comparison between prediction and measurement for flow over the fence (Re = 82.5): □, experimental data; —, WACEB; – –, QUICK; · – · –, UPWIND.

APPENDIX A. NOMENCLATURE

A	coefficients in Equation (7)
F	total fluxes across the cell faces
H	height of channel
j_{ij}, q_{ij} ($i = 1, 3$ and $j = 1, 3$)	transformation factor

J	determinant of Jacobian
L	length of cavity
Re	Reynolds number
s	height of fence
S_Φ, S_C, S^{CD}, S^{DC}	source terms
u, v, w	Cartesian velocity components
U_m	mean velocity in the channel
U, V, W	contravariant velocity components
x, y, z	Cartesian co-ordinates

Greek letters

ξ, η, ζ	generalized curvilinear co-ordinates
κ	weighted-average coefficient
Φ	dependent variable
Γ	diffusion coefficient

Superscripts

n	iteration level
$\sim$	normalized value

Subscripts

f (= e,w,n,s,t,b)	value at the cell faces
F (= E,W,N,S,T,B)	value at the nodes

APPENDIX B

The cross-diffusion source term in Equation (2) is defined as

$$S^{CD} = \frac{1}{J}\frac{\partial}{\partial\xi}\left(\frac{\Gamma_\Phi}{J}(q_{21}\Phi_\eta + q_{31}\Phi_\zeta)\right) + \frac{1}{J}\frac{\partial}{\partial\eta}\left(\frac{\Gamma_\Phi}{J}(q_{12}\Phi_\xi + q_{32}\Phi_\zeta)\right) + \frac{1}{J}\frac{\partial}{\partial\zeta}\left(\frac{\Gamma_\Phi}{J}(q_{13}\Phi_\xi + q_{23}\Phi_\eta)\right)$$

The transformation coefficients are defined as follows:

$$j_{11}=\frac{\partial y}{\partial \eta}\frac{\partial z}{\partial \zeta}-\frac{\partial y}{\partial \zeta}\frac{\partial z}{\partial \eta}, \qquad j_{12}=\frac{\partial y}{\partial \zeta}\frac{\partial z}{\partial \xi}-\frac{\partial y}{\partial \xi}\frac{\partial z}{\partial \zeta}, \qquad j_{13}=\frac{\partial y}{\partial \xi}\frac{\partial z}{\partial \eta}-\frac{\partial y}{\partial \eta}\frac{\partial z}{\partial \xi}$$

$$j_{21}=\frac{\partial x}{\partial \zeta}\frac{\partial z}{\partial \eta}-\frac{\partial x}{\partial \eta}\frac{\partial z}{\partial \zeta}, \qquad j_{22}=\frac{\partial x}{\partial \xi}\frac{\partial z}{\partial \zeta}-\frac{\partial x}{\partial \zeta}\frac{\partial z}{\partial \xi}, \qquad j_{23}=\frac{\partial x}{\partial \eta}\frac{\partial z}{\partial \xi}-\frac{\partial x}{\partial \xi}\frac{\partial z}{\partial \eta}$$

$$j_{31}=\frac{\partial x}{\partial \eta}\frac{\partial y}{\partial \zeta}-\frac{\partial x}{\partial \zeta}\frac{\partial y}{\partial \eta}, \qquad j_{32}=\frac{\partial x}{\partial \zeta}\frac{\partial y}{\partial \xi}-\frac{\partial x}{\partial \xi}\frac{\partial y}{\partial \zeta}, \qquad j_{33}=\frac{\partial x}{\partial \xi}\frac{\partial y}{\partial \eta}-\frac{\partial x}{\partial \eta}\frac{\partial y}{\partial \xi}$$

and

$$q_{ij}=\sum_{k=1}^{3} j_{ki}j_{kj}, \quad i=1,3, \quad j=1,3.$$

REFERENCES

1. Price HS, Varga RS, Warren JE. Application of oscillation matrices to diffusion-correction equations. *Journal of Mathematics and Physics* 1966; **45**: 301–311.
2. Leonard BP. A stable and accurate convective modelling procedure based on quadratic upstream interpolation. *Computational Methods and Applications in Mechanical Engineering* 1979; **19**: 59–98.
3. Zhu J, Leschziner MA. A local oscillation-damping algorithm for higher-order convection schemes. *Computational Methods and Applications in Mechanical Engineering* 1988; **67**: 355–366.
4. Leonard BP. Simple high-accuracy resolution program for convective modelling of discontinuities. *International Journal for Numerical Methods in Fluids* 1988; **8**: 1291–1318.
5. Gaskell PH, Lau AKC. Curvature-compensated convective transport: SMART, a new boundedness preserving transport algorithm. *International Journal for Numerical Methods in Fluids* 1988; **8**: 617–641.
6. Zhu J. On the higher-order bounded discretization schemes for finite volume computations of incompressible flows. *Computational Methods and Applications in Mechanical Engineering* 1992; **98**: 345–360.
7. Zhu J. A low-diffusive and oscillation-free convection scheme. *Communications in Applied Numerical Methods* 1991; **7**: 225–232.
8. Khosla PK, Rubin SG. A diagonally dominant second-order accurate implicit scheme. *Computers and Fluids* 1974; **2**: 207–209.
9. Rhie CM, Chow WL. A numerical study of the turbulent flow past an isolated airfoil with trailing edge separation. *AIAA Journal* 1983; **21**: 1525–1532.
10. Patankar SV. *Numerical Heat Transfer and Fluid Flow*. McGraw-Hill: New York, 1980.
11. Carvalho MG, Durst F, Pereira JC. Predictions and measurements of laminar flow over two-dimensional obstacles. *Applied Mathematical Modelling* 1987; **11**: 23–34.

